Acta Oceanol. Sin., 2023, Vol. 42, No. 10, P. 127–136
https://doi.org/10.1007/s13131-023-2231-5
http://www.aosocean.com
E-mail: ocean2@hyxb.org.cn

Contributions of annual and semiannual tidal constituents to chart datum in the China seas and adjacent waters

Yikai Feng[1], Yanguang Fu[1]*, Long Yang[1], Dongxu Zhou[1]

[1] First Institute of Oceanography, Ministry of Natural Resources, Qingdao 266061, China

Received 23 March 2023; accepted 27 June 2023

Abstract

Global uniform chart datum (CD) surface construction is the basic upon which to realize various vertical datums transformation, and is of great importance for geospatial data expression under the same vertical datum. Generally, the CD level is computed by developing the function between tidal constituents' harmonic constants and time, i.e., the lowest astronomical tide is taken as the lowest predicted tide level by adopting the major constituents over a 19-a period. The CD surface prescribed in China is the theoretical lowest tide (TLT) and is calculated using 13 tidal constituents, i.e., short -period (Q_1, O_1, P_1, K_1, N_2, M_2, S_2, K_2, M_4, MS_4 and M_6) and long-period (Sa and Ssa) tidal constituents. Although the accuracy in determining short-period tidal constituents has improved gradually, the long-period tide has not been studied thoroughly owing to nonstationary and temporal variations. Previous studies have intended to evaluate the effect of Sa and Ssa tides in the determination of the TLT level for the purpose of determining a more accurate CD surface for the China seas and adjacent waters. Here, the parameters of long-period tidal correction and long-period tidal correction rate were treated as the effect of both Sa and Ssa on the TLT, and the TOPEX/Poseidon and Jason series satellite altimetry data ranged from October 1992 to April 2022 were adopted to analyze the contribution of long-period tidal constituents. Results showed that the average long-period correction value is 10.10 cm (range from 8.57 cm to 14.98 cm), and that the average long-period tidal contribution rate is 14.56% (range from 9.09% to 23.97%) in the China seas and adjacent waters. Finally, data from 82 tide gauge station with at least a 1-a record of hourly observations were compared with satellite-derived result. We concluded that the long-period tidal contribution should not be neglected in TLT construction. Furthermore, to reduce tidal datum uncertainty, accurate extraction of long-period tidal constituents should receive closer attentions.

Key words: tidal datum, chart datum, long-period tidal constituent, lowest normal low water, China seas and adjacent waters

Citation: Feng Yikai, Fu Yanguang, Yang Long, Zhou Dongxu. 2023. Contributions of annual and semiannual tidal constituents to chart datum in the China seas and adjacent waters. Acta Oceanologica Sinica, 42(10): 127–136, doi: 10.1007/s13131-023-2231-5

1 Introduction

As sea level changes globally, accurate determination of the ocean tidal datum plays an increasingly important role in analysis of sea level variation, ocean depth determination and vertical datum unification (Gill and Schultz, 2001; Slobbe et al.,2018). Generally, tidal datum is constructed by adopting tidal constants extracted from tide gauge measurements, satellite altimetry data, and tide models (El-Diasty, 2020). However, with increasing focus of accurate extraction of short-period tidal constituents, i.e., the diurnal and semidiurnal tidal constituents, the contribution of the long-period tidal constituents has not been received adequate attention in the past studies despite its importance in the determination of the tidal datum.

Different types of tidal datums, such as the lowest astronomical tide (LAT), mean lower low water, and theoretical lowest tide (TLT), have been adopted as chart datum (CD) in various countries to determine horizontal boundaries and provide accurate vertical references for bathymetry (Wu et al., 2019). Modern tidal datum construction is based on ocean tide models. The near-continuous digital expression of a CD is achieved using grid model with high-resolution geographic locations, and the accuracy of a datum model depends mainly on the tide model. For example, the US-based Vertical Datum Transformation project used a regional ocean tide model to establish the mean lower low water surface (Parker et al., 2003; Yang et al., 2010). The UK and Eire Vertical Offshore Reference Frames project produced an inlaid tide model that combined a regional and global ocean tide model to establish a corresponding LAT model (Iliffe et al., 2013). Although the advantage of the inlaid tidal model is that it improves the accuracy of the diurnal and semidiurnal tidal constituents, the LAT value does not consider the effects of long-period tidal constituents. Some earlier studies on global ocean tide model assessment (Cheng and Andersen, 2011; Lyard et al., 2021; Egbert and Erofeeva, 2002), analyzed the accuracy of the performance of short-period tidal constituents (i.e., diurnal of semi-diurnal tidal constituents), but did not conduct similar assessment of long-period tidal constituents (Shum et al., 1997; Stammer et al., 2014). Consequently, accurate extraction of long-period tidal constituents has not received sufficient attention.

Satellite altimetry data can provide a continuous, high spatial

Foundation item: The National Natural Science Foundation of China under contract No. 42104035; the Basic Scientific Fund for National Public Research Institutes of China under contract No. 2023Q05; the Natural Science Foundation of Shandong Province under contract No. ZR2020QD087.

*Corresponding author, E-mail: ygfu@fio.org.cn

resolution sea-level height time series with near global coverage that allows for accurate evaluation of the spatiotemporal characteristics of long-period tidal constituents (Yuan et al., 2023). However, satellite altimetry observations show poor accuracy performance because of the land–sea interactions (Guo et al., 2022) and inaccurate geophysical correction models in coastal areas (Andersen and Scharroo, 2011). In recent years, satellite altimetry has made great progress both in reducing instrument error and an improving data processing and correction models (Pascual et al., 2009), which make it a more feasible approach for obtaining a reasonable spatial distribution of reliable long-period tidal constituents. Recently, Handoko et al. (2017) and Fu et al. (2020b) conducted detailed evaluation of the main geophysical corrections to derive accurate sea surface heights in the Indonesian seas and the South China Sea, respectively. Owing to its current accuracy and maturity, altimetry is considered a fully operational observation system dedicated to scientific and operational applications, and it is increasingly applied to research investigating the precision of short-period tidal constituents (Fu et al., 2020a; Wei et al., 2022; Daher et al., 2015). For example, Fang et al. (2004) used a 10-a series of TOPEX/Poseidon (T/P) along-track altimetry data to derive the semidiurnal, diurnal, and long-period tides in the China seas and adjacent waters, and highlighted that sea level observation conducted over a period of at least several years is necessary to obtain reliable long-period tidal harmonic constants. Harmonic analyses of 16-a long time series of T/P and Jason-1 altimeter data were conducted to study the 18.6-a nodal constituent (Cherniawsky et al., 2010). Additionally, T/P-Jason-1-Jason-2 primary mission along-track data collected over almost 20 a were used to derive four principal tidal constituents (M_2, S_2, K_1, and O_1) (Cheng et al., 2016) and eight diurnal and semidiurnal mean tide constituents (Daher et al., 2015). However, the contributions of long-period tidal constituents to tidal datums remain rarely studied (Yusof et al., 2017).

Long-period tides (e.g., 8 d, 2 weeks, 1 month, 6 months and 18.6 a) have been studied since the late 19th century (Wunsch, 1967). The long-period tidal correction, i.e., that for annual (Sa) and semiannual (Ssa) tidal constituents, is a component of the CD used in China. However, most global tide models do not provide tidal constants of Sa and Ssa, except for the FES2014, NAO99b (Matsumoto et al., 2000), and EOT 20 (Hart-Davis et al., 2021) models, and the Sa and Ssa tidal constituents provided by those models are the simulation results of pure fluid dynamics (amplitude < 1 cm). The large differences between tide model results and tide gauge observations limit the use of tide model results. Thus, investigates of the spatial distribution of the long-period tidal contribution should rely on combined use of satellite-derived retrievals and tide gauge observations.

The China seas and adjacent waters, i.e., the Bohai Sea, Yellow Sea, East China Sea, and South China Sea, have different tidal properties such as diurnal, semidiurnal, and mixed tides that make them among the most complex tidal waters globally. Recently, Ke et al. (2020) calculated an LAT seamless CD model based on tidal constants derived from the Atlantic Ocean 2008 model. In Li et al. (2020), the FES2014 global tide model was adopted to construct the TLT and LAT datum model, and statistical analysis was performed on the distribution of the datum values of TLT and LAT. Unfortunately, these studies did not consider the contributions of long-period tidal constituents when constructing the CD surface.

The aim of this study was to investigate the contributions of long-period tidal constituents to the TLT in the China seas and adjacent waters. Accordingly, the remainder of the paper is structured as follows. Section 2 presents the data and methodology used for determining the TLT. Section 3 investigates the regional variability of the long-period tidal constituents extracted from satellite altimetry and tide gauge observations. Section 4 analyzes the magnitude of the long-period tidal contributions to TLT. Section 5 discusses in detail the reasons for the tidal contribution differences between tide gauge observations and satellite-derived results. Finally, Section 6 presents the derived conclusions.

2 Materials and methods

2.1 *Tide gauge data*

The dataset of harmonic constants used in this study comprised observations obtained from 82 tide gauge stations. Data from 61 stations comprised Global Extreme Sea Level Analysis version 2 (GESLA-2) tide gauge records (Piccioni et al., 2019), and the data from the remaining 21 stations comprised privately collected Chinese tide gauge (CTG) observations. Geographic information pertaining to the CTG is listed in Table 1, and Fig. 1 displays the locations of all the tide gauge stations.

The GESLA-2 tide gauge records, distributed on a quasi-global scale, are freely available from the PANGAEA repository (http://www.gesla.org). The GESLA-2 tide gauge database contains 39 148 a of sea level data from 1 355 stations with at least a 1-a record of hourly (or more frequent) sea level observations (Woodworth et al., 2016). The harmonic constants were obtained, the least squares method was used, with the criterion of the minimum period of the observations of each record must be larger than 1 a and the maximum length of temporal gaps were below 30%. The 61 stations used in this paper contain 1 379 a of tide gauge observations, Fig. 2 displays a histogram of the time length of the tidal observations at each of the 61 stations.

The period of hourly observations sampled at each of the CTG stations extended from January 1, 2010 to December 31, 2012. The tidal harmonic constants of the tidal constituents, i.e., Q_1, O_1, P_1, K_1, N_2, M_2, S_2, K_2, M_4, MS_4, M_6, Sa, and Ssa, were derived from harmonic analysis of the observations (Ruiz-Etcheverry et al., 2015). During the harmonic analysis, missing observations were not filled through interpolation because interpolation methods can distort the results of the spectral analysis of water level records. The amplitude and Greenwich phase value of the Sa and Ssa tidal constituents at each CTG station are listed in Table 1.

2.2 *Satellite altimetry data*

We used satellite-derived sea level height data from the T/P, Jason-1, Jason-2, and Jason-3 missions covering from October 1992 to April 2022, acquired from the Radar Altimeter Database System (http://rads.tudelft.nl), which provides a harmonized, validated, and cross-calibrated set of altimeter data (Scharroo et al., 2013). The 30-a-long altimetric time series allow precise determination of annual-period tidal constituents.

We referred to the literature regarding the impact of the altimeter corrections of tidal height variations when applying different models for a given geographical correction. Table 2 presents a summary of the chosen models and the corrections applied to obtain tidal heights from the altimeter record that coincide with the default corrections of the Radar Altimeter Database System. We applied various environmental corrections (wet and dry tropospheric corrections, ionospheric correction, and sea state bias) and geophysical corrections (polar tide, solid earth tide and load tide corrections), but ignored the inverse barometer correction to ensure consistency with the tide gauge records. The tidal constants of the 13 tidal constituents mentioned above were then estimated directly through harmonic analysis of each single along-track tidal time series using the S_TIDE toolbox (Pan et al., 2018).

Table 1. Geographical information and harmonic constants of annual (Sa) and semiannual (Ssa) long-period tidal constituents at the Chinese tidal gauge stations

Station No.	Latitude	Longitude	Sa				Ssa			
			Amplitude/cm	Amplitude_err/cm	Phase	Phase_err	Amplitude/cm	Amplitude_err/cm	Phase	Phase_err
1	40.30°N	122.10°E	29.12	2.66	201.39°	5.44°	2.89	2.38	32.40°	52.58°
2	39.82°N	124.15°E	27.55	2.72	207.66°	5.83°	3.21	2.31	28.94°	49.13°
3	39.23°N	122.67°E	26.06	2.99	208.31°	11.45°	2.22	2.88	8.46°	31.01°
4	39.21°N	119.01°E	28.27	2.28	204.85°	4.76°	2.79	3.21	352.59°	44.48°
5	38.98°N	117.78°E	29.75	2.10	203.27°	10.51°	3.51	1.80	342.81°	19.70°
6	38.92°N	118.51°E	27.52	2.27	203.63°	10.18°	3.18	2.39	344.52°	38.74°
7	37.83°N	120.74°E	24.82	2.45	210.42°	2.08°	1.39	2.48	346.74°	53.38°
8	37.65°N	120.32°E	25.12	2.15	209.95°	5.45°	1.47	2.18	331.86°	78.95°
9	36.87°N	122.42°E	22.15	2.11	215.09°	6.37°	1.72	1.91	2.79°	47.21°
10	36.27°N	121.38°E	22.38	3.01	216.26°	11.97°	1.48	2.73	351.93°	31.51°
11	30.83°N	121.83°E	19.77	2.15	227.49°	5.44°	2.52	1.97	6.50°	85.80°
12	29.22°N	121.97°E	16.55	2.98	244.01°	11.50°	2.69	2.96	38.39°	33.42°
13	28.69°N	121.47°E	14.19	2.27	253.30°	5.06°	3.76	2.01	23.76°	89.55°
14	26.92°N	120.22°E	13.61	2.78	274.62°	10.96°	4.38	2.56	57.26°	36.11°
15	25.47°N	119.83°E	13.22	2.03	283.79°	8.64°	4.61	2.26	55.42°	17.03°
16	24.88°N	118.95°E	15.07	2.91	296.64°	11.98°	4.87	2.62	60.15°	30.16°
17	23.40°N	117.10°E	13.06	1.79	301.71°	5.08°	5.27	1.71	57.36°	68.61°
18	23.22°N	116.78°E	13.00	2.27	302.15°	8.59°	5.67	2.33	59.45°	52.76°
19	21.02°N	109.12°E	10.01	3.07	273.42°	6.16°	6.03	3.25	86.63°	48.57°
20	20.23°N	110.13°E	10.54	1.42	292.42°	9.10°	6.29	1.46	76.82°	14.69°
21	18.23°N	109.50°E	14.45	2.02	315.19°	4.75°	7.50	2.16	69.13°	60.72°

Note: err represents standard error.

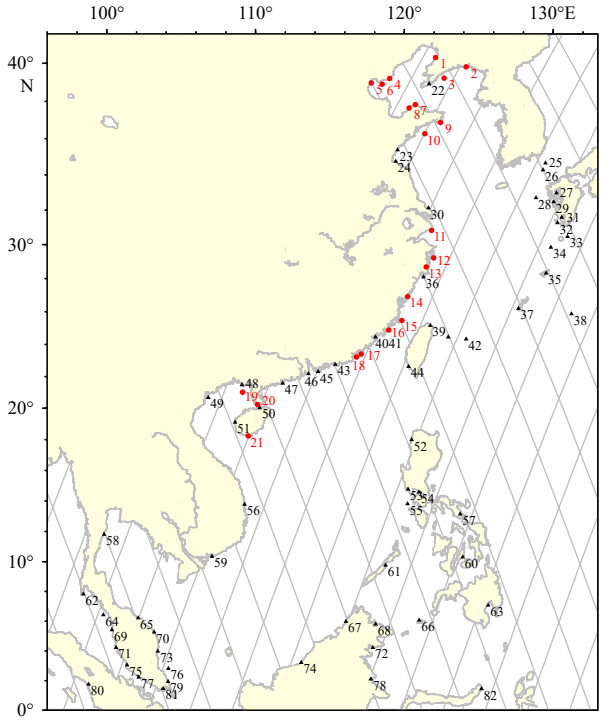

Fig. 1. Tide gauge station distribution in the China seas and adjacent waters. Red dots indicate the Chinese tide gauge stations considered in this study, black triangles identity locations of the GESLA-2 stations, and solid gray lines indicate the TOPEX/Poseidon and Jason primary mission tracks.

Owing to the phenomenon of tidal aliasing caused by the relationship between the frequency of the tidal constituents and the sampling period of the sea level data (i.e., the sampling period was approximately 9.915 6 d for the T/P satellite), a longer time series was needed to separate the tidal constituents (Schlax and Chelton, 1994). The length of the record of satellite-derived sea level data required to separate the 13 tidal constituents in the T/P-Jason observations can be determined based on the Rayleigh criterion (Table 3). The longest record of T/P satellite data required to fully separate Ssa and K_1 is 9.19 a, which was calculated using the s_minimumLOR function in the S_TIDE toolbox. The period of 9.19 a is obviously less than the 30-a record of the T/P-Jason satellite data used in this study. Therefore, the 13 tidal constituents can be guaranteed to be fully resolved.

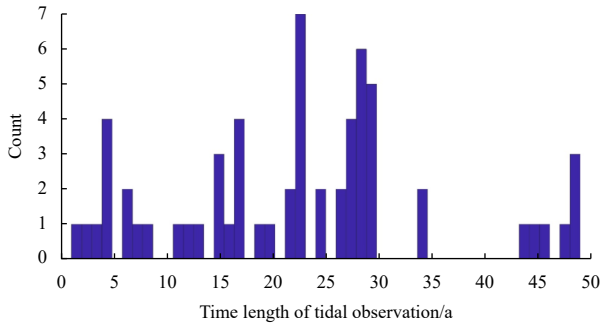

Fig. 2. Histogram of the time length of tidal observations at the GESLA-2 tide gauge stations.

2.3 *China's chart datum determination*

The TLT has been adopted as the CD of the China seas and adjacent waters. According to the relevant regulations of the Marine Surveying and Mapping Institute of the People's Liberation Army Navy (State Administration for Market Regulation and Standardization Administration of the People's Republic of China, 2022), the TLT was calculated using diurnal and semidi-

Table 2. Geographical correction models used for tidal constituent analysis

Geography correction	Edit criteria		Description
	min/m	max/m	
Dry tropospheric correction	–2.40	–2.10	ECMWF dry tropospheric correction
Wet tropospheric correction	–0.60	0.00	radiometer wet tropospheric correction
Ionospheric correction	–0.04	0.04	smoothed dual-frequency ionospheric correction
Solid earth tide	–1.00	1.00	Elastic response to tidal potential
Load tide	–0.50	0.50	FES2014a load tide

Table 3. Length of TOPEX/Poseidon satellite-derived data required to fully separate the 13 tidal constituents (unit: a)

Constituent	Ssa	Q_1	O_1	P_1	K_1	N_2	M_2	S_2	K_2	M_4	MS_4	M_6
Sa	1.00	0.23	0.14	0.32	0.90	0.16	0.21	0.19	0.31	0.09	1.51	0.06
Ssa		0.31	0.17	0.47	9.19	0.19	0.26	0.24	0.45	0.10	0.60	0.06
Q_1			0.37	0.87	0.32	0.47	1.62	1.04	0.96	0.15	0.20	0.08
O_1				0.26	0.17	1.63	0.47	0.57	0.27	0.27	0.13	0.10
P_1					0.50	0.31	0.56	0.47	9.19	0.13	0.27	0.07
K_1						0.19	0.27	0.24	0.47	0.10	0.56	0.06
N_2							0.67	0.87	0.32	0.23	0.14	0.10
M_2								2.94	0.60	0.17	0.18	0.09
S_2									0.50	0.18	0.17	0.09
K_2										0.13	0.26	0.07
M_4											0.09	0.17
MS_4												0.06

urnal (Q_1, O_1, P_1, K_1, N_2, M_2, S_2 and K_2), shallow-water (M_4, MS_4 and M_6), and long-period (Sa and Ssa) tidal constituents, by the following equation:

$$\begin{aligned} \mathrm{TLT} = &-\min[(fH)_{K_1}\cos\phi_{K_1} + (fH)_{K_2}\cos(2\phi_{K_1}+a_4) - R_1 - \\ &R_2 - R_3 + (fH)_{M_4}\cos\phi_{M_4} + (fH)_{MS_4}\cos\phi_{MS_4} + \\ &(fH)_{M_6}\cos\phi_{M_6} + H_{Ssa}\cos\phi_{Ssa} - H_{Sa}\left|\cos\phi_{Sa}\right|], \end{aligned} \tag{1}$$

where TLT is the CD value, H and f are the amplitude and focus factor of each tidal constituent. The TLT is the one variable function of ϕ_{K_1}, which ranges from 0° to 360°. The minimum value of this function is the TLT. Among which, L_{long} is the long-period tidal contribution:

$$L_{long} = H_{Ssa}\cos\phi_{Ssa} - H_{Sa}\left|\cos\phi_{Sa}\right|. \tag{2}$$

According to the equilibrium relationship between tidal components, the following approximate hypothesis is introduced:

$$\begin{cases} R_1 = \sqrt{((fH)_{M_2})^2 + ((fH)_{O_1})^2 + 2(fH)_{M_2}(fH)_{O_1}\cos(\phi_{K_1}+a_1)} \\ R_2 = \sqrt{((fH)_{S_2})^2 + ((fH)_{P_1})^2 + 2(fH)_{S_2}(fH)_{P_1}\cos(\phi_{K_1}+a_2)} \\ R_3 = \sqrt{((fH)_{N_2})^2 + ((fH)_{Q_1})^2 + 2(fH)_{N_2}(fH)_{Q_1}\cos(\phi_{K_1}+a_3)} \end{cases}, \tag{3}$$

$$\begin{cases} a_1 = g_{K_1} + g_{O_1} - g_{M_2} \\ a_2 = g_{K_1} + g_{P_1} - g_{S_2} \\ a_3 = g_{K_1} + g_{Q_1} - g_{N_2} \\ a_4 = 2g_{K_1} - 180° - g_{K_2} \end{cases}, \tag{4}$$

where g is the phase of each tidal constituent. In calculation of the TLT, the f value of each tidal constituent was determined depending on the tidal regime, specific calculation process can be referred to Standardization Administration of China (State Administration for Market Regulation and Standardization Administration of the People's Republic of China, 2022).

3 Regional variability of long-period tidal constituents

3.1 *Temporal variability*

Different from short-period tidal constituents, i.e., M_2 and K_1, that have relatively stable amplitude and phase, the long-period tidal constituents of Sa and Ssa are nonstationary and show substantial temporal variation (Feng et al., 2015).

To assess the temporal variability of Sa and Ssa, long-term observations (1988–2011) from 22 of the 82 tide gauge stations were selected. First, tests were performed by adopting continuous records of time series data of six different lengths, i.e., 1 a and 2 a, 3 a, 5 a, 10 a, and 18 a. Then, the amplitude and phase of each of the 13 tidal constituents were obtained through harmonic analysis for each individual time series and the TLT value was calculated. Table 4 lists the maximum difference, minimum difference, and standard error of Sa and Ssa amplitude and the TLT value, difference refers to the difference between results obtained from tidal observations at different time scales and the mean.

It can be seen from Table 4 that the Sa and Ssa constituents obtained from annual scale tidal observations have greatest instability, mainly because the period of Sa is 1 a; thus, the annual-scale tidal level data only just meet the requirement of its shortest period. For tidal observations on the 2-a time scale, the obtained values of Sa and Ssa both show a reasonable degree of improvement, e.g., the standard error of Sa is increased from 2.69 cm to 1.79 cm. When the time scale reaches 10 a, the standard error of Sa and Ssa is only 0.60 cm and 0.43 cm, respectively, with very high accuracy. However, it is virtually impossible for most tide gauge stations to obtain continuous tidal measurements over a period of more than a decade. The results show that the longer the time scale of the observation record, the more stable the derived long-period tidal harmonic constant. To reduce the influence of temporal variability, a time series record with length of at least 3 a is required for extraction of adequate long-period tidal constituents.

3.2 *Spatial variability*

The China seas and adjacent waters can be divided into four regions: the Bohai Sea (38°–41°N, 119°–127°E), Yellow Sea

Table 4. Differences in amplitude (cm) of long-period tidal constituents and theoretical lowest tide (TLT) value obtained from time series records of different time scales

Continuous time length	Sa			Ssa			TLT		
	min	max	err	min	max	err	min	max	err
1 a	−8.53	9.94	2.69	−5.77	5.15	1.95	−26.80	19.06	5.69
2 a	−7.25	5.08	1.79	−4.56	3.67	1.37	−26.76	18.61	5.09
3 a	−6.40	4.51	1.44	−2.70	3.15	1.09	−23.80	18.12	4.72
5 a	−3.46	3.18	1.06	−1.99	2.54	0.89	−12.38	14.47	4.22
10 a	−2.05	1.99	0.60	−1.27	1.25	0.43	−8.34	7.40	2.81
18 a	−1.06	0.74	0.29	−0.57	0.76	0.19	−1.48	1.68	0.43

Note: err represents standard error.

(33°–38°N, 117°–126°E), East China Sea (23°–33°N, 117°–131°E), and South China Sea (0°–23°N, 100°–122°E). As described in Section 2.2, time series records of sea level change from October 1992 to April 2022 were derived from T/P-Jason series satellite altimetry data, from which Sa and Ssa tidal constants were calculated for 7 961 along-track points by adopting the harmonic analysis method.

The spatial distributions of the satellite-derived along-track values of amplitude and phase of the Sa and Ssa tidal constituents are presented in Fig. 3. It can be seen that the long-period tidal harmonic constants have marked spatial variability. For example, the maximum value of Sa amplitude of 26.24 cm is in the Bohai Sea, with 57.3% and 17.9% of the along-track points below 10 cm and above 15 cm, respectively. The magnitude of Ssa amplitude is smaller than that of Sa amplitude, i.e., the maximum value is 7.40 cm, with 86.1% of the along-track points below 3 cm. In the China seas and adjacent waters, the average amplitude of the Sa and Ssa tidal constituents is in the range of 8.08–15.82 cm and 1.86–2.21 cm, respectively. It should be noted that the number of along-track satellite points located in each of the four regions of the China seas and adjacent waters varied, which will have affected the statistical results, i.e., there were 219, 458, 1 268, and 6 016 along-track points in the Bohai Sea, Yellow Sea, East China Sea, and South China Sea, respectively.

We observed that the long-period tidal amplitude showed gradual change spatially, with smaller magnitudes in deep open-ocean areas. It is suggested that the large spatial differences and gradual spatial gradients in satellite-derived long-period tidal constituents contribute to spatial variability in the CD.

Furthermore, the water depth of 200 m was taken as the dividing line, and the water depth data was from the ETOPO1 model (https://www.ncei.noaa.gov/products/etopo-global-relief-model). The study area was divided into offshore and deep-sea areas. The statistics of amplitude values of Sa and Ssa were shown in Fig. 4.

It can be seen from Fig. 4 that the amplitude values showed large magnitude in the offshore area than the deep-sea area for both Sa and Ssa constituents, and these two long-period tidal constituents displayed consistent spatial distribution of amplitude in offshore and deep-sea area respectively. From the perspective of mathematical statistics, the average amplitude value of Sa in offshore and deep-sea area is 10.36 cm and 5.65 cm, respectively, and for Ssa is 2.65 cm and 1.82 cm, respectively.

In the offshore area, the amplitude values of Sa in 76% of along-track points range from 5 cm to 15 cm, but for Ssa constituent, 79% points are below 4 cm. Combined with Fig. 3, we can see that the large values are mainly located in the Bohai Sea, South China Sea and Gulf of Thailand. In contrast to offshore waters, the vast majority of along-track points are located in deep-sea area, where more reliable satellite-derived results can be extracted. In deep-sea area, the amplitude values of Sa in 80% of points range from 2 cm to 8 cm, and for Ssa constituent, 66% points are below 2 cm.

Tide gauge stations provide sea level height values with high accuracy and high resolution. In recent studies, tide gauge obser-

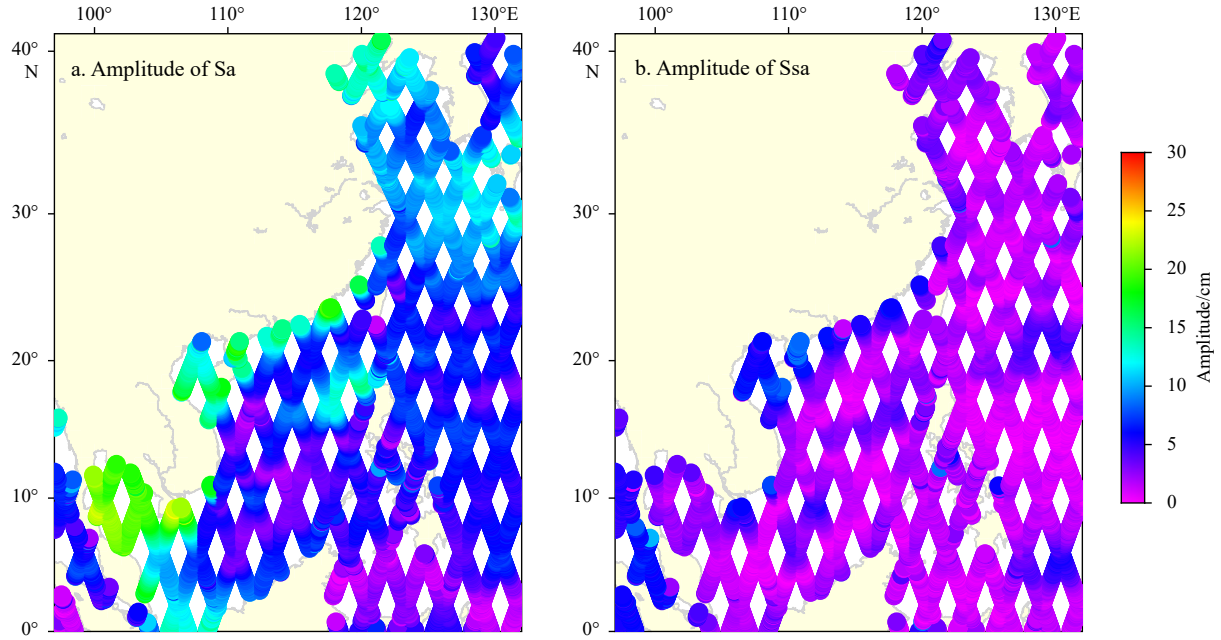

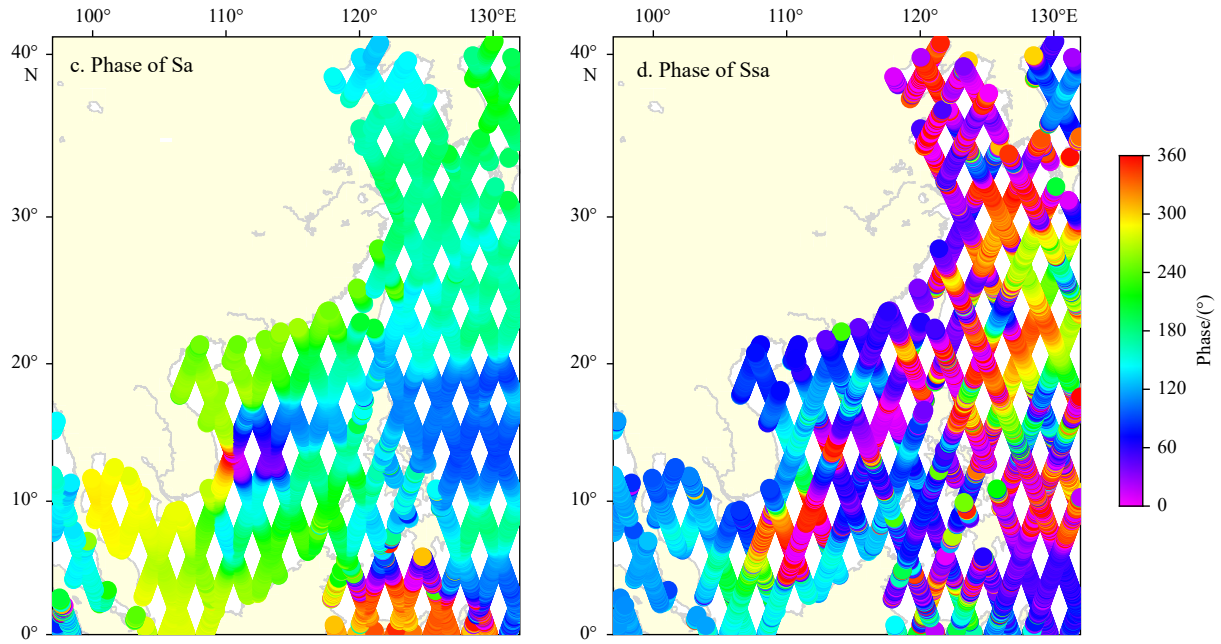

Fig. 3. Satellite-derived tidal amplitudes and phase values of annual (Sa) and semiannual (Ssa) long-period tidal constituents.

vations have been regarded as "true" data with which to evaluate satellite-derived or model-derived tidal constants. The 18.61-a time series is ideal for obtaining true tidal constants based on the Rayleigh criterion for tidal constituent separation. A record of at least one full year of tide gauge observations is required for obtaining the Sa tidal constituent, although this might include large inaccuracies in the data. Finally, we obtained long-period tidal constants of the Sa and Ssa tidal constituents at the 82 tide gauge stations, and their amplitude and phase are presented in Fig. 5.

In comparison with the satellite-derived results, the amplitude of Sa derived from the tide gauge data varies over a larger scale (0.64 – 29.75 cm). However, the amplitude of Ssa is more restricted (0.67 – 8.16 cm). The large differences observed in Sa and Ssa are mainly the result of their behavior in coastal sea areas. Comparison of the tide gauge records and the nearest satellite altimetry grid point data is discussed in Section 5.

4 Magnitude of tidal contributions to TLT

The long-period tidal constituent corrections (LTCs) and contribution rates (LTCRs) were calculated for each satellite along-track point and each tide gauge using Eq. (1). The LTCR refers to the percentage of the LTC in the TLT.

The satellite-derived results were interpolated onto a 15′ × 15′ grid using the inverse distance weighting method, and the spatial distribution of the LTCR is shown in Fig. 6. The largest LTCRs are found in the Gulf of Thailand, northeastern South China Sea,

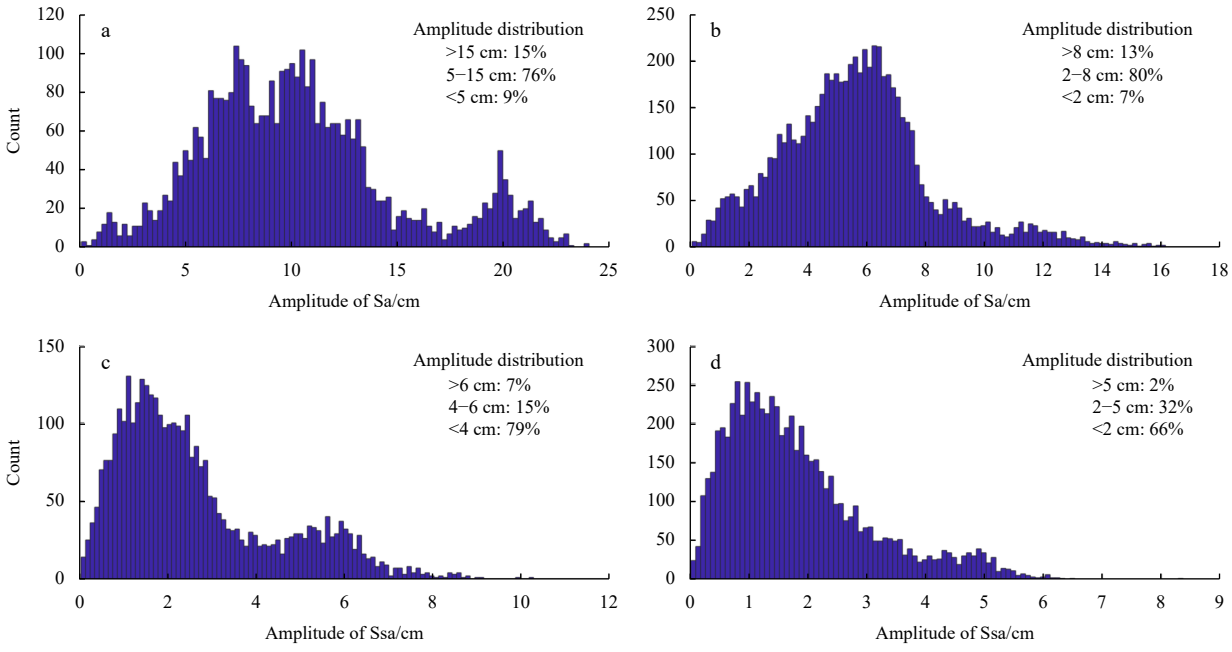

Fig. 4. Statistics of amplitude values of annual (Sa) and semiannual (Ssa) in offshore (depth < 200 m, a and c) and deep-sea (depth > 200 m, b and d) area.

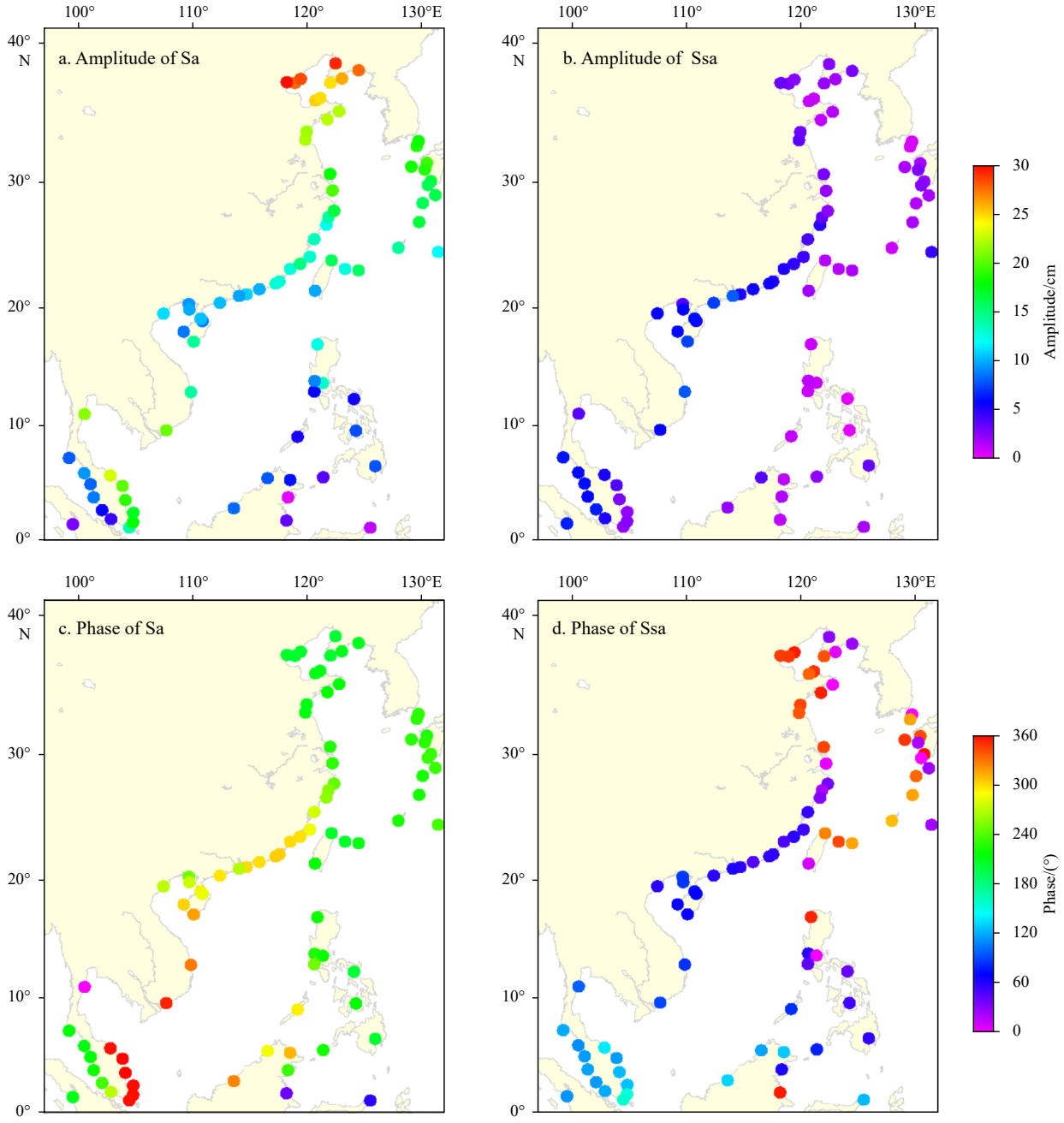

Fig. 5. Long-period tidal constants of annual (Sa) and semiannual (Ssa) tidal constituents at the 82 tide gauge stations.

and Japan Sea (East Sea). According to statistics of the valid along-track points, 82.1% of the LTCs are in the range of 5–20 cm, 2.5% of the LTCs are >20 cm, and 15.4% of the LTCs are <5 cm.

To investigate the relative performance of the LTC in relation to the four regions of the China seas and adjacent waters, histograms of the LTCs are presented in Fig. 7 and further results are listed in Table 5. In the Bohai Sea, the LTCR of approximately 71.2% of along-track points is >20%, the average LTCR is 24.0%. Additionally, the average LTC is 14.98 cm. The LTCR is remarkable in this area, which might reflect the large amplitude of Sa. In the Yellow Sea, East China Sea, and South China Sea, the average LTRCs are 15.06%, 10.12%, and 9.09%, respectively. It should be noted that some of the variation among the regions is attributable to the different numbers of along-track points in the four different regions of the China seas and adjacent waters.

The TLT is calculated using three types of tidal constituent: major (diurnal and semidiurnal), shallow-water and long-period constituents. Our data showed that these three types of correction have different contribution rates in the China seas and adjacent waters. The maximum average value of the LTCR is up to 23.97% in the Bohai Sea; average LTCR in the entire study area is 14.56%.

5 Discussion

Assessment of the accuracy of the satellite-derived long-period tidal constituents was performed by comparing the results from the 82 tide gauge stations with the nearest satellite along-track point data. Figure 7 illustrated the relationship of the tidal amplitude difference between tide gauge observations and the satellite-derived results. The difference in Sa amplitude is in the range of –5.27 cm to 14.73 cm, and 48.8% of the difference values are < 10 cm (average value is 5.65 cm; standard deviation value is

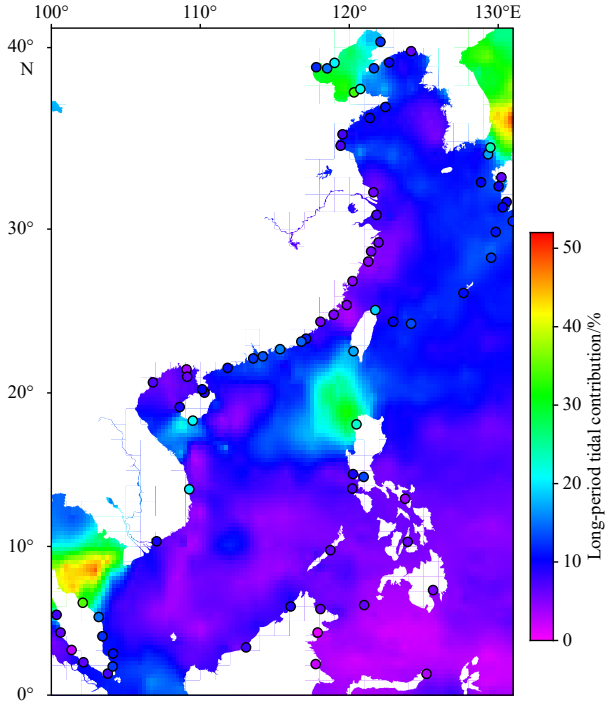

Fig. 6. Spatial distribution of satellite-derived long-period tidal contributions. Colored dots depict results from the tide gauge stations.

4.23 cm). The difference in Ssa amplitude is between –2.31 cm and 6.50 cm, with 73.2% of values within ±2 cm (average value is 1.02 cm; standard deviation value is 1.70 cm).

It is evident that the difference in Sa amplitudes is larger at higher latitudes (Fig. 8a). For example, the amplitude difference is in the range of –0.72–11.44 cm at 29.22–34.65°N and in the range of –0.19–13.38 cm at north of 34.75°N. The positive values indicate that the amplitude differences are larger in the tide gauge results than in the satellite-derived results. Figure 8b shows the amplitude difference as a function of distance between a tide gauge station and the nearest satellite along-track point. Distances range from 2.91 km to 261.28 km, although significant correlation between them was not found.

Figure 9 compares the LTCR between the tide gauge results and the satellite-derived results. The difference between them ranges from –40.59% to 14.33%, with 80.5% of stations within ±5%. The maximum LTCR value is 34.18% (Station 65, see Fig. 1) and the second-highest value is in the Yellow Sea (Station 8, 33.78%). An interesting phenomenon is that although these two stations show the largest LTCR value, the long-period tidal amplitude of each of these stations is not the largest compared with that of surrounding stations. For example, Station 5 shows the largest amplitude of 29.75 cm, with an LTC value of 27.22 cm, but the LTRC value is only 11.98%.

6 Conclusions

Multi-mission satellite altimetry data and tide gauge observations were used to study the contribution of long-period tidal

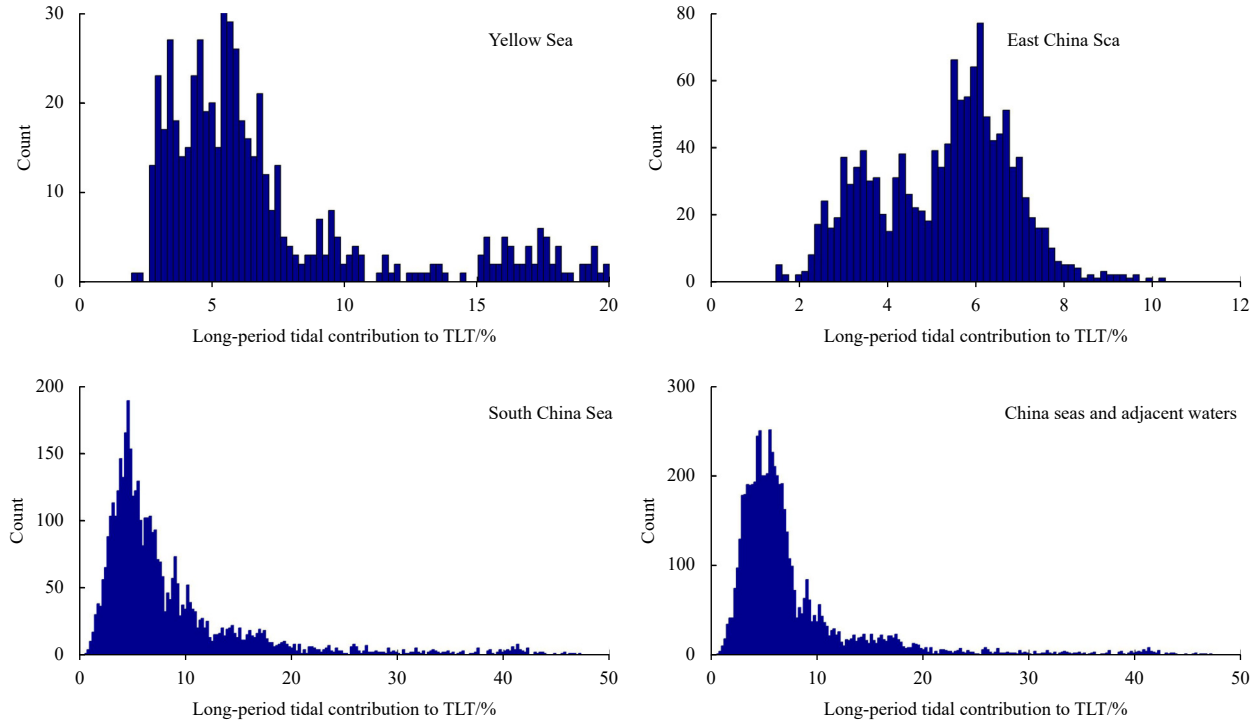

Fig. 7. Distribution of the long-period tidal constituent contributions to the theoretical lowest tide (TLT).

Table 5. Average contribution of three types of tidal constituents to the theoretical lowest tide in the four regions of the China seas and adjacent waters

Sea area	Eight major constituents contribution/%	Shallow water tidal contribution/%	Long-period tidal contribution/%
Bohai Sea	77.08	2.18	23.97
Yellow Sea	85.78	1.96	15.06
East China Sea	91.80	0.63	10.12
South China Sea	92.87	1.28	9.09

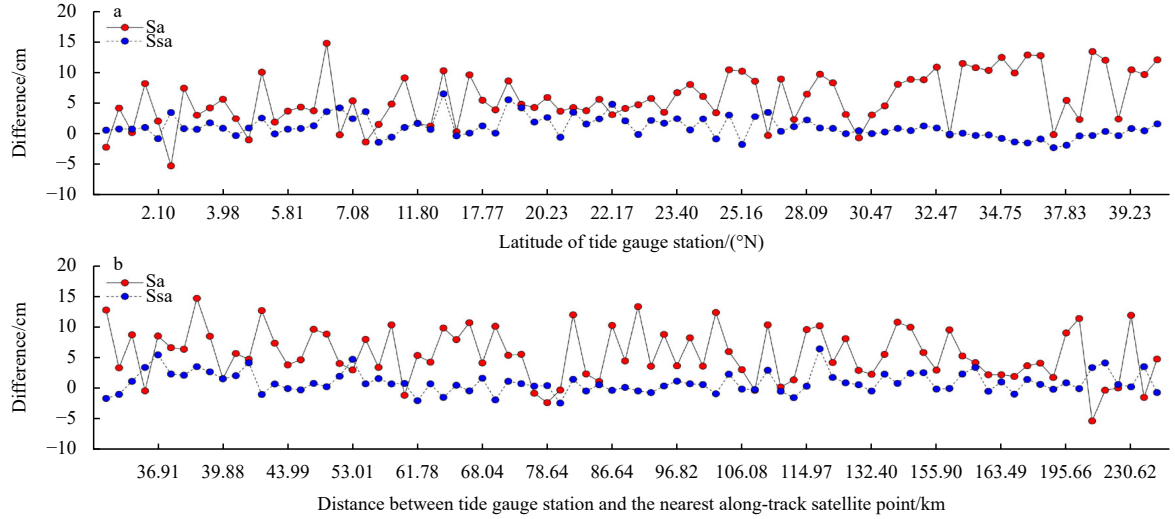

Fig. 8. Annual (Sa) and semiannual (Ssa) tidal amplitude differences as a function of the latitude of the tide gauge stations (a), and the distance between the tide gauge stations and the nearest satellite along-track point (b).

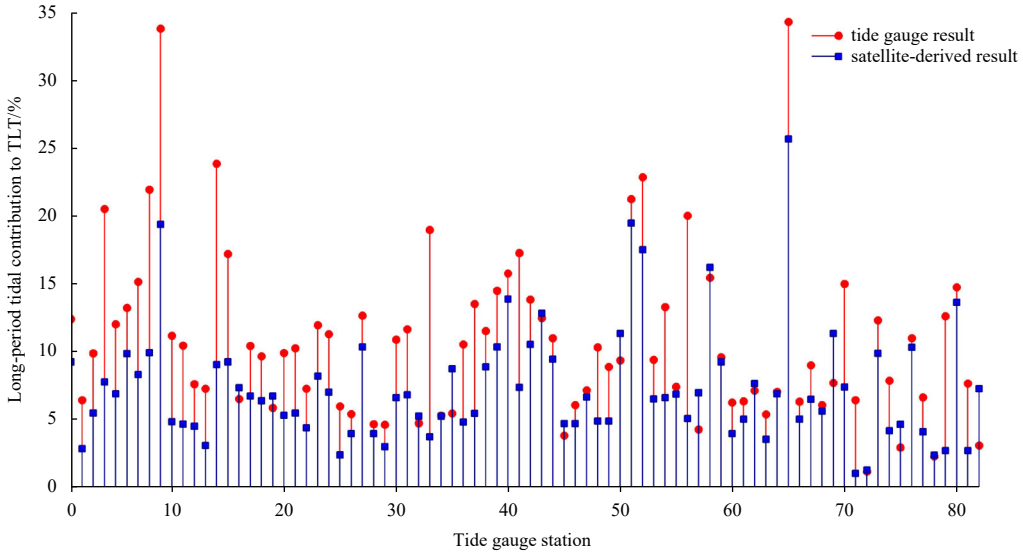

Fig. 9. Comparison of long-period tidal contributions between tide gauge results and satellite-derived results.

constituents to the TLT in the China seas and adjacent waters. The TLT was calculated using 13 different tidal constituents (Q_1, O_1, P_1, K_1, N_2, M_2, S_2, K_2, M_4, MS_4, M_6, Sa and Ssa) and a long-period tidal correction was performed by combining the Sa and Ssa tidal constituents.

A tidal height time series extending for almost 30 a derived from the T/P and Jason series satellite altimetry data, but without inverse barometric correction to ensure consistency with the tide gauge results. First, we found that the maximum amplitudes of the satellite-derived along-track Sa and Ssa tidal constituent were 31.13 cm and 12.38 cm, respectively. The average amplitudes of Sa and Ssa in the China seas and adjacent waters were 9.39 cm and 1.95 cm, respectively. We analyzed the LTC and LTCR of the satellite-derived results, which revealed that the average LTC and LTCR values in the study area were 10.10 cm and 14.56%, respectively.

In the four regions of the China seas and adjacent waters, the average LTC value was largest in the Bohai Sea (23.97%) and smallest in the East China Sea (9.09%); the derivation of this parameter was affected by the total number of along-track points in the different regions. The amplitudes of Sa and Ssa obtained from the 82 tide gauge observations were range of 0.64–29.75 cm and 0.67–8.16 cm, respectively. The low precision of satellite altimetry data in coastal areas is the main factor that contributes to the differences between the tide gauge data and the satellite-derived results. Comparisons of the differences in the LTC values between the observations from the 82 tide gauge stations and the satellite-derived results indicated that long-period tidal correction is vital to the establishment of the TLT. Therefore, precise extraction of long-period tidal constituents will be the focus of our future research.

Acknowledgements

The authors would like to acknowledge the Radar Altimeter Database System for providing the multi-mission satellite altimetric data and correction models.

References

Andersen O B, Scharroo R. 2011. Range and geophysical corrections in coastal regions: and implications for mean sea surface de-

termination. In: Vignudelli S, Kostianoy A G, Cipollini P, et al. , eds. Coastal Altimetry. Berlin, Heidelberg: Springer-Verlag, 103–145, doi: 10.1007/978-3-642-12796-0_5

Cheng Yongcun, Andersen O B. 2011. Multimission empirical ocean tide modeling for shallow waters and polar seas. Journal of Geophysical Research: Oceans, 116(C11): C11001, doi: 10.1029/2011JC007172

Cheng Yongcun, Xu Qing, Zhang Yuan. 2016. Tidal estimation from TOPEX/Poseidon, Jason Primary, and interleaved missions in the Bohai, Yellow, and East China seas. Journal of Coastal Research, 32(4): 966–973, doi: 10.2112/JCOASTRES-D-14-00209.1

Cherniawsky J Y, Foreman M G G, Kang S K, et al. 2010. 18.6-year lunar nodal tides from altimeter data. Continental Shelf Research, 30(6): 575–587, doi: 10.1016/j.csr.2009.10.002

Daher V B, de Oliveira Vieira Paes R C, França G B, et al. 2015. Extraction of tide constituents by harmonic analysis using altimetry satellite data in the Brazilian coast. Journal of Atmospheric and Oceanic Technology, 32(3): 614–626, doi: 10.1175/JTECH-D-14-00091.1

Egbert G D, Erofeeva S Y. 2002. Efficient inverse modeling of barotropic ocean tides. Journal of Atmospheric and Oceanic Technology, 19(2): 183–204, doi: 10.1175/1520-0426(2002)019<0183:EIMOBO>2.0.CO;2

El-Diasty M. 2020. Optimal lowest astronomical tide estimation using maximum likelihood estimator with multiple ocean models hybridization. ISPRS International Journal of Geo-Information, 9(5): 327, doi: 10.3390/ijgi9050327

Fang Guohong, Wang Yonggang, Wei Zexun, et al. 2004. Empirical cotidal charts of the Bohai, Yellow, and East China seas from 10 years of TOPEX/Poseidon altimetry. Journal of Geophysical Research: Oceans, 109(C11): C11006, doi: 10.1029/2004JC002484

Feng Xiangbo, Tsimplis M N, Marcos M, et al. 2015. Spatial and temporal variations of the seasonal sea level cycle in the Northwest Pacific. Journal of Geophysical Research: Oceans, 120(10): 7091–7112, doi: 10.1002/2015JC011154

Fu Yanguang, Feng Yikai, Zhou Dongxu, et al. 2020a. Accuracy assessment of global ocean tide models in the South China Sea using satellite altimeter and tide gauge data. Acta Oceanologica Sinica, 39(12): 1–10, doi: 10.1007/s13131-020-1685-y

Fu Yanguang, Zhou Dongxu, Zhou Xinghua, et al. 2020b. Evaluation of satellite-derived tidal constituents in the South China Sea by adopting the most suitable geophysical correction models. Journal of Oceanography, 76(3): 183–196, doi: 10.1007/s10872-019-00537-2

Gill S K, Schultz J R. 2001. Tidal Datums and their Applications. Silver Spring, MD, USA: NOAA

Guo Jinyun, Hwang C, Deng Xiaoli. 2022. Editorial: Application of satellite altimetry in marine geodesy and geophysics. Frontiers in Earth Science, 10: 910562, doi: 10.3389/feart.2022.910562

Handoko E Y, Fernandes M J, Lázaro C. 2017. Assessment of altimetric range and geophysical corrections and mean sea surface models—Impacts on sea level variability around the Indonesian seas. Remote Sensing, 9(2): 102, doi: 10.3390/rs9020102

Hart-Davis M G, Piccioni G, Dettmering D, et al. 2021. EOT20: a global ocean tide model from multi-mission satellite altimetry. Earth System Science Data, 13(8): 3869–3884, doi: 10.5194/essd-13-3869-2021

Iliffe J C, Ziebart M K, Turner J F, et al. 2013. Accuracy of vertical datum surfaces in coastal and offshore zones. Survey Review, 45(331): 254–262, doi: 10.1179/1752270613Y.0000000040

Ke Hao, Li Fei, Ai Songtao, et al. 2020. Establishment of chart datum and vertical datum transformation for hydrography in the Chinese Great Wall Bay, Antarctic Peninsula. Journal of Surveying Engineering, 146(2): 05020003, doi: 10.1061/(ASCE)SU.1943-5428.0000312

Li Jie, Fu Yanguang, Tang Qiuhua, et al. 2020. Accuracy assessment of a seamless depth datum model established on the basis of the global ocean tide model. Journal of Coastal Research, 99(S1): 74–78, doi: 10.2112/SI99-011.1

Lyard F H, Allain D J, Cancet M, et al. 2021. FES2014 global ocean tide atlas: design and performance. Ocean Science, 17(3): 615–649, doi: 10.5194/os-17-615-2021

Matsumoto K, Takanezawa T, Ooe M. 2000. Ocean tide models developed by assimilating TOPEX/POSEIDON altimeter data into hydrodynamical model: a global model and a regional model around Japan. Journal of Oceanography, 56(5): 567–581, doi: 10.1023/A:1011157212596

Pan Haidong, Lv Xianqing, Wang Yingying, et al. 2018. Exploration of tidal-fluvial interaction in the Columbia River estuary using S_TIDE. Journal of Geophysical Research: Oceans, 123(9): 6598–6619, doi: 10.1029/2018JC014146

Parker B, Milbert D, Hess K, et al. 2003. National VDatum—the implementation of a national vertical datum transformation database. Sea Technology, 44(9): 10–15

Pascual A, Boone C, Larnicol G, et al. 2009. On the quality of real-time altimeter gridded fields: comparison with *in situ* data. Journal of Atmospheric and Oceanic Technology, 26(3): 556–569, doi: 10.1175/2008JTECHO556.1

Piccioni G, Dettmering D, Bosch W, et al. 2019. TICON: Tidal Constants based on GESLA sea-level records from globally located tide gauges. Geoscience Data Journal, 6(2): 97–104, doi: 10.1002/gdj3.72

Ruiz-Etcheverry L A, Saraceno M, Piola A R, et al. 2015. A comparison of the annual cycle of sea level in coastal areas from gridded satellite altimetry and tide gauges. Continental Shelf Research, 92: 87–97, doi: 10.1016/j.csr.2014.10.006

Scharroo R, Leuliette E, Lillibridge J, et al. 2013. RADS: Consistent multi-mission products. In: Symposium on 20 Years of Progress in Radar Altimetry. Venice, Italy: ESA

Schlax M G, Chelton D B. 1994. Aliased tidal errors in TOPEX/POSEIDON sea surface height data. Journal of Geophysical Research: Oceans, 99(C12): 24761–24775, doi: 10.1029/94JC01925

Shum C K, Woodworth P L, Andersen O B, et al. 1997. Accuracy assessment of recent ocean tide models. Journal of Geophysical Research: Oceans, 102(C11): 25173–25194, doi: 10.1029/97JC00445

Slobbe D C, Sumihar J, Frederikse T, et al. 2018. A Kalman filter approach to realize the lowest astronomical tide surface. Marine Geodesy, 41(1): 44–67, doi: 10.1080/01490419.2017.1391900

Stammer D, Ray R D, Andersen O B, et al. 2014. Accuracy assessment of global barotropic ocean tide models. Reviews of Geophysics, 52(3): 243–282, doi: 10.1002/2014RG000450

State Administration for Market Regulation, Standardization Administration of the People's Republic of China. 2022. GB12327-2022 Specifications for hydrographic survey (in Chinese). Beijing: Standards Press of China

Wei Zexun, Pan Haidong, Xu Tengfei, et al. 2022. Development history of the numerical simulation of tides in the East Asian marginal seas: An overview. Journal of Marine Science and Engineering, 10(7): 984, doi: 10.3390/jmse10070984

Woodworth P L, Hunter J R, Marcos M, et al. 2016. Towards a global higher-frequency sea level dataset. Geoscience Data Journal, 3(2): 50–59, doi: 10.1002/gdj3.42

Wu Wei, Myers E, Shi Lei, et al. 2019. Modeling tidal datums and spatially varying uncertainty in the Texas and western Louisiana coastal waters. Journal of Marine Science and Engineering, 7(2): 44, doi: 10.3390/jmse7020044

Wunsch C. 1967. The long-period tides. Reviews of Geophysics, 5(4): 447–475, doi: 10.1029/RG005i004p00447

Yang Zizang, Myers E P, White S A. 2010. VDatum for eastern Louisiana and Mississippi coastal waters: tidal datums, marine grids, and sea surface topography. In: NOAA Technical Memorandum NOS CS 19. Silver Spring, Maryland, USA: National Oceanic and Atmospheric Administration

Yuan Jiajia, Guo Jinyun, Zhu Chengcheng, et al. 2023. SDUST2020 MSS: a global 1′ × 1′ mean sea surface model determined from multi-satellite altimetry data. Earth System Science Data, 15(1): 155–169, doi: 10.5194/essd-15-155-2023

Yusof N H M, Mahmud M R, Abdullah M H. 2017. Effect of long term tidal constituents on mean sea level trend during El-Niño and La-Niña phenomena. The International Archives of the Photogrammetry, Remote Sensing and Spatial Information Sciences, XLII-4/W5: 225–234